

SCATTERED RADIATION FROM OBSCURED QUASARS IN DISTANT RADIO GALAXIES

HIEN D. TRAN,¹ MARSHALL H. COHEN,² PATRICK M. OGLE,² ROBERT W. GOODRICH,³ AND
SPERELLO DI SEREGO ALIGHIERI⁴

Received 1997 August 18; accepted 1998 January 27

ABSTRACT

We present optical spectropolarimetric and imaging polarimetric observations of four high-redshift radio galaxies (HzRGs) obtained with the Low Resolution Imaging Spectrometer of the 10 m Keck I telescope. A broad Mg II λ 2800 emission line is detected in the total and polarized flux spectra of 3C 265 and 3C 277.2. The fractional polarization is high, and both it and the position angle are constant with wavelength after accounting for dilution by unpolarized starlight of the host galaxy, which can contribute substantially. An extended unpolarized continuum similar to that observed in other active galactic nuclei is also detected. Imaging polarimetry reveals a rough double-fan morphology of the polarized light coincident with the extended aligned emission regions, with the position angle essentially perpendicular to the radial structure of the extended UV/optical emission and with the degree of polarization increasing with radius away from the nucleus. The radio jets lie inside the extended emission regions and, like every radius, are roughly perpendicular to the polarization position angle. These results strengthen the view that powerful radio galaxies would be called quasars if viewed from the proper direction. Based on the polarimetric data presented in this paper and in previous studies, scattering of radiation from an obscured quasar source appears to be the preferred interpretation over jet-induced star formation for explaining the alignment effect in HzRGs. Both electrons and dust can play a major role in the scattering process. However, the lack of strong direct evidence for either case and our ignorance of the properties and distribution of the scatterers in these galaxies make it very difficult to discriminate between the two. Our data reveal a chance alignment of 3C 343.1 with a foreground galaxy, which dominates the observed optical flux from the system.

Subject headings: galaxies: active — galaxies: jets — polarization — quasars: general — radio: continuum: galaxies — scattering

1. INTRODUCTION

Distant radio galaxies ($z \gtrsim 1.0$) offer a powerful laboratory for probing cosmology and galactic evolution because they are extragalactic objects that are spatially extended and visible at large look-back times. They are also important because they appear to be related to quasars (based on the radio galaxy/quasar unification model; e.g., Barthel 1989), thus providing important insights into understanding the nature of this most powerful class of objects in the universe. The discovery that many distant radio galaxies show extended emission-line- and UV-continuum-emitting regions that are often aligned with the radio structure axis (the “alignment effect;” see McCarthy 1993 for a review) means that this phenomenon must be understood before these galaxies can be used as probes of cosmology and galactic evolution. Several suggestions have been put forward to account for this effect. They include star formation resulting from the interaction of the radio jets with the interstellar medium (De Young 1981, 1989; Chambers, Miley, & Joyce 1988; Rees 1989) and alternatively, nuclear light scattered by dust or electrons (e.g., Tadhunter et al. 1992; Cimatti et al. 1993; di Serego Alighieri, Cimatti, & Fosbury 1994). Another, poorly investigated possibility is

that the extended emission represents the illumination pattern of a Doppler-beamed continuum, analogous to that seen directly in blazars. Other mechanisms are also possible (see, e.g., Daly 1992), but currently these are the main contenders. Polarimetric observations showing that the extended emission is highly polarized, with the polarization position angle (P.A.) perpendicular to the radio structure axis (e.g., Jannuzi & Elston 1991; Tadhunter et al. 1992; Cimatti et al. 1993; di Serego Alighieri et al. 1994), offer strong support for the scattering pictures but do not totally exclude star formation. For example, a large amount of dust associated with star-forming regions along the jets could also give rise to scattering of radiation from the central nucleus in the jet-induced star formation scenario. There have also been other arguments for this picture (e.g., Best, Longair, & Röttgering 1996, 1997).

If the scattering picture is correct, we expect the extended light to be highly polarized, and when combined with the radio galaxy/quasar hypothesis, we also expect to see a quasar spectrum in polarized light. Just such a picture indeed has been shown to be the case in some of the low-redshift radio galaxies (i.e., 3C 234: Antonucci 1984; Tran, Cohen, & Goodrich 1995; 3C 321: Young et al. 1996; Cygnus A: Ogle et al. 1997). Tran et al. also showed that the radio galaxy 3C 234 would be indistinguishable from a quasar if it were not for the high amount of obscuration in the nucleus, and a similar result was found for 3C 109 (Goodrich & Cohen 1992). A similar unification model based on obscuration/orientation effects has been well-established for Seyfert 1 and 2 galaxies (e.g., Antonucci & Miller 1985; Miller & Goodrich 1990; Tran 1995a, 1995b, 1995c). Recent observational evidence is mounting that the

¹ Institute of Geophysics and Planetary Physics, Lawrence Livermore National Laboratory, 7000 East Avenue, P.O. Box 808, L-413, Livermore, CA 94550; htran@igpp.llnl.gov.

² Palomar Observatory, California Institute of Technology, Pasadena, CA 91125; mhc@astro.caltech.edu, pmo@astro.caltech.edu.

³ CARA/Keck Observatory, 65-1120 Mamalahoa Highway, Kamuela, HI 96743; goodrich@keck.hawaii.edu.

⁴ Osservatorio Astrofisico di Arcetri, Firenze, Italy; sperello@arcetri.astro.it.

TABLE 1
LOG OF POLARIMETRIC OBSERVATIONS

Object	UT Date	Mode ^a	Exposure (s)	Slit P.A. (deg)
3C 265.....	1994 Dec 31	SPOL	4 × 2310	142
	1995 Jan 28	SPOL	4 × 2400	134
	1995 Jun 1	IPOL	4 × 1620	...
3C 277.2.....	1996 Apr 17	SPOL	4 × 2400	90
	1996 Apr 16	IPOL	4 × 1260	...
3C 324.....	1995 Jul 28	IPOL	8 × 900	...
3C 343.1.....	1995 Jul 29	SPOL	4 × 1800	90

^a SPOL = spectropolarimetry; IPOL = imaging polarimetry.

same picture may also apply to many high-redshift radio galaxies (HzRGs) (di Serego Alighieri et al. 1994; Dey & Spinrad 1996; Cimatti et al. 1996, 1997; Cohen et al. 1996; Dey et al. 1996) based on the detection of the broad Mg II λ 2800 line in either the total flux spectra or polarized flux spectra. A convincingly detected broad Mg II line in the polarized flux spectrum would demonstrate that the quasar scattering hypothesis and the obscuration/reflection picture are at least partly responsible for the alignment effect and that radio galaxies may be quasars viewed from an equatorial direction. Di Serego Alighieri et al. (1994) and Cimatti et al. (1996, 1997) have presented evidence for broad Mg II in the polarized-flux spectra of some of these galaxies, but these results are based on fairly low signal-to-noise ratio (S/N) data, and further study is needed.

Alternatively, if the extended continuum represents scattering of a Doppler-beamed source, the polarized light should consist predominantly of continuum, with little or no emission lines. We expect significant Doppler beaming in all quasars, as quasars viewed from polar directions are thought to appear as blazars. A hybrid of the last two scenarios is likely, in which the scatterers see a normal quasar spectrum with some contribution, especially in the polar directions, by a beamed continuum. Ultimately, one might hope to constrain beaming models via spatially resolved spectropolarimetry.

While the mechanism responsible for the polarized light in these HzRGs is generally thought to be scattering, the nature of the scatterers continues to be a source of debate. At issue is whether scattering by electrons or dust dominates, although it is recognized that *both* could be present in producing the observed polarization. The nature of the scattering agents could have some important implications on the alignment effect and nature of these galaxies. For example, if it can be conclusively shown that electron scattering is primarily responsible for the extended polarized light, it would provide an argument against jet-induced star formation as the main cause of the alignment effect, since this picture predicts that dust grains that are abundant within the star-forming regions in the jet streams would be the principal medium for scattering the light.

In this paper, we investigate a number of HzRGs using the Keck I 10 m telescope to address various issues relating to the alignment effect, the nature of the scatterers, and the radio galaxy/quasar unification hypothesis. In particular, we look for the signature of broad Mg II in polarized flux and map the polarization structure of the extended emission in order to investigate the central nucleus and the geometry of the scattering process. We discuss the implications of these observations on the above issues. Our sample of

objects comprises those with previously detected polarizations: 3C 265, 3C 277.2, and 3C 343.1, which are slightly brighter and have relatively smaller redshifts ($z \sim 0.8$) than those ($z \sim 1.4$) studied by Dey et al. (1996) and Cimatti et al. (1996, 1997) (3C 13, 3C 256, 3C 324, and 3C 356), and our study complements the previous work. We also use imaging polarimetry to study 3C 324.

Section 2 describes the observations. In § 3 we present our data analysis and results of the spectro- and imaging polarimetry. The discussion and interpretation of these results are presented in § 4, and a summary and conclusions in § 5.

2. OBSERVATIONS

Our observations were carried out at the W. M. Keck Observatory using the 10 m telescope with the polarimeter (Cohen et al. 1997) installed in the Low Resolution Imaging Spectrometer (Oke et al. 1995). A 1" wide, long slit was centered on the nucleus of the galaxy and oriented along the UV extensions. A 300 grooves mm^{-1} grating provided a dispersion of $2.5 \text{ \AA pixel}^{-1}$ and a resolution of $\sim 10 \text{ \AA}$ (FWHM). The spectropolarimetric observations were performed following standard procedures of rotating the half-wave plate to four position angles and calibrating the instruments with null and standard polarization stars (see Cohen et al. 1997 for details). No second-order blocking filter was used in these observations, but we observed the flux-standard stars both with and without a GG495 filter, which blocks all light with $\lambda < 4950 \text{ \AA}$, to correct for any second-order light. The residual second-order effects are small and apply only to the spectral regions $\geq 7500 \text{ \AA}$. They do not affect the conclusions drawn in this paper.

Table 1 shows the log of the observations. The choice of objects was based on their relatively high apparent brightness ($m_V < 22$), high polarization from surveys published in the literature (Cimatti et al. 1993), or display of a dramatic alignment effect. To improve the S/N, multiple observations of the same object were carried out at different epochs, and the individual results were co-added and are presented here as the final form.

In addition to spectropolarimetry, we also obtained imaging polarimetric observations for three galaxies: 3C 265, 2C 277.2, and 3C 324. The imaging polarimetry used procedures identical to those employed in spectropolarimetry, except they were made through either a standard *B* or *V* filter, with no slit, and with a mirror replacing the grating. Data reductions were carried out using the imaging processing software VISTA as described by Tran et al. (1995) and Cohen et al. (1997).

3. RESULTS AND ANALYSIS

3.1. 3C 265

Of all the HzRGs that we observed, 3C 265 ($z = 0.811$) is the brightest ($m_V = 20.9$) and has by far the best S/N data. We thus focus our discussion and analysis on this object. The total flux spectrum of 3C 265 in the spectral region around Mg II has been discussed by Dey & Spinrad (1996). The nuclear spectrum, shown in Figure 1, is typical of a narrow-line radio galaxy (NLRG), displaying many emission lines with a wide range in strengths, ionizations, and atomic species (compare, for example, to the spectrum of 3C 234; Tran et al. 1995). In Table 2 we list the measured emission-line ratios (relative to H β) and the observed equiv-

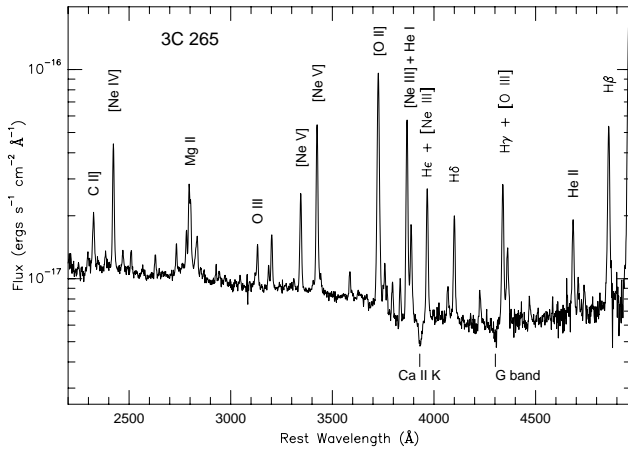


FIG. 1.—Total flux spectrum of the nucleus of 3C 265, plotted in logarithmic scale to show faint features. Note the presence of broad Mg II emission and the stellar absorption features.

alent widths (EWs) from the nuclear spectra of 3C 265, along with those of 3C 277.2 and 3C 343.1. Except for 3C 343.1, these measurements were made from the observed spectrum without removing the host starlight. Detailed analysis of these spectrophotometric measurements in relation to dust, electron scattering, and photoionization models will be the subject of a later paper.

In Table 2, we identify several faint UV lines that are rarely observed in a HzRG. These include [Mg VII] $\lambda\lambda$ 2509, 2629 (equivalents of [O III] $\lambda\lambda$ 4959, 5007 in the same iso-electronic sequence), [Mg V] $\lambda\lambda$ 2783, 2928 (equivalents of [O I] $\lambda\lambda$ 6300, 6364), as well as other lines due to permitted He II and O III resonance-fluorescence. We identify a weak, broad component due to the resonance-fluorescence line O III λ 3444 at the base of [Ne V] λ 3426.

Dey & Spinrad (1996) identified the emission line blueward of Mg II $\lambda\lambda$ 2796, 2805 as [Mg VII] λ 2786. It is more likely, however, that this line is actually [Mg V] λ 2783

TABLE 2
OBSERVED LINE FLUX RATIOS AND EQUIVALENT WIDTHS

LINE	3C 265		3C 277.2		3C 343.1 ^a	
	Flux Ratio ^b	EW	Flux Ratio ^b	EW	Flux Ratio ^b	EW
C III λ 2297	0.0389	3.10
C II] λ 2326	0.233	19.5	0.1345	16.1
He II λ 2386	0.0458	3.78	0.0327	4.01
[Ne IV] λ 2424	0.560	46.34	0.3905	44.15
[O II] λ 2470	0.0624	5.28
He II λ 2512 + [Mg VII] λ 2509	0.0560	5.24	0.0608	7.96
[Na VI] λ 2569 ?	0.0533	4.85
[Mg VII] λ 2629	0.0654	6.00	0.0438	5.85
He II λ 2733	0.0634	5.38	0.0637	8.34
[Mg V] λ 2783	0.0721	5.47	0.0617	7.00
Mg II (b + n) $\lambda\lambda$ 2796, 2805	0.774	74.0	0.311	41.1	0.179	56.8
He I 2830 + O III λ 2836	0.130	11.0	0.0601	7.73
[Ar IV] λ 2854	0.0185	1.65
[Ar IV] λ 2868	0.0147	1.36
[Mg V] λ 2928	0.0240	2.27
He I λ 2946	0.0208	1.96
O III λ 3047	0.0264	2.65	0.023:	2.8:
O III λ 3133	0.1385	14.05	0.0842	10.30
He I λ 3188 + He II λ 3203	0.177	18.0	0.118	14.22
He I λ 3188	0.0442	4.46
He II λ 3203	0.134	13.5
[Ne V] λ 3346	0.3105	32.0	0.2814	33.43
[Ne V] λ 3426 + O III λ 3444	0.883	93.5	0.778	92.3	0.0342	7.28
[Fe VII] λ 3588	0.0585	6.53	0.011:	1.3:
[O II] λ 3727	1.801	230.0	1.676	235.2	2.031	432.4
H12 + H11 $\lambda\lambda$ 3750, 3771	0.143	18.94	0.0916	13.3
H10 λ 3798	0.0532	7.35	0.0430	6.41
H9 λ 3835	0.0559	8.02	0.0359	5.47
[Ne III] λ 3869 + H8 + He I	1.130	159.17	0.413	93.8
[Ne III] λ 3869 + He I λ 3868	0.910	128.8	0.817	125.5
H8 + He I λ 3889	0.248	35.3	0.123	19.0
Ca II K absorption	-0.0517	-7.4
He + [Ne III] λ 3967	0.387	55.12	0.360	52.7	0.203	42.5
[S II] λ 4071	0.0713	10.24	0.0412	5.78	0.272	51.1
H δ	0.287	41.76	0.229	31.8	0.114	21.5
[Fe V] λ 4227	0.0787	12.30	0.029:	4.0:
H γ	0.4722	71.7	0.3445	48.7
[O III] λ 4363	0.2018	30.40	0.157	21.9
He I λ 4471	0.0347	5.01
He II λ 4686	0.273	37.0	0.293	35.5
[Ar IV] λ 4712	0.0667	9.06
[Ar IV] λ 4740	0.0543	7.36
H β	1.000	121.59	1.000	110.0	1.000	117.7
[O III] λ 4959	3.7	494.0	3.856	370.6	0.746	75.3
[O III] λ 5007	11.67	995.5	2.21	200.0

^a Flux ratios and EWs are measured from galaxy-subtracted spectrum.

^b Flux ratio relative to H β ; colons denote uncertainty $\geq 20\%$.

(Osterbrock 1963, 1997). Since the two [Mg VII] lines $\lambda\lambda 2509$ and 2629 have been identified in our spectrum and they are analogous to the strong [O III] $\lambda\lambda 4959, 5007$ ubiquitous in nebular spectra, it is unlikely that there is a third [Mg VII] line stronger than these two. Furthermore, the [Mg V] $\lambda 2783$ is equivalent to [O I] $\lambda 6300$ in the same isoelectronic sequence, and if its identification is correct, we would expect to see the analog of [O I] $\lambda 6364$ in [Mg V] at $\lambda 2928$ with about one-third intensity ratio. Such a line is indeed present with about the correct intensity ratio (see Table 2). Thus, there is little doubt that the emission line at 2783 \AA is correctly identified with [Mg V]. Its identification shows that the very wide range of ionization in 3C 265 is continuous. The feature just to the red of the Mg II doublet has a stubby profile, which suggests that it is not a single line but is probably a doublet. We identify it as the blend He I $\lambda 2830$ + O III $\lambda 2836$.

In Figure 1, broad wings in Mg II can clearly be seen in the total flux spectrum. A least-squares fit of multiple Gaussian profiles to the Mg II emission-line complex is shown in Figure 2. The FWHM of the broad Mg II in total flux is $11,000 \pm 700 \text{ km s}^{-1}$, which is similar to but somewhat broader than that measured by Dey & Spinrad (1996). The spectropolarimetry of the nuclear region of 3C 265 is shown in Figure 3. The observed fractional polarization P (Fig. 3b) is high, rising smoothly from 6% in the red (rest frame blue) to $\sim 12\%$ in the blue (rest frame UV). Broad Mg II emission is clearly present in the polarized flux spec-

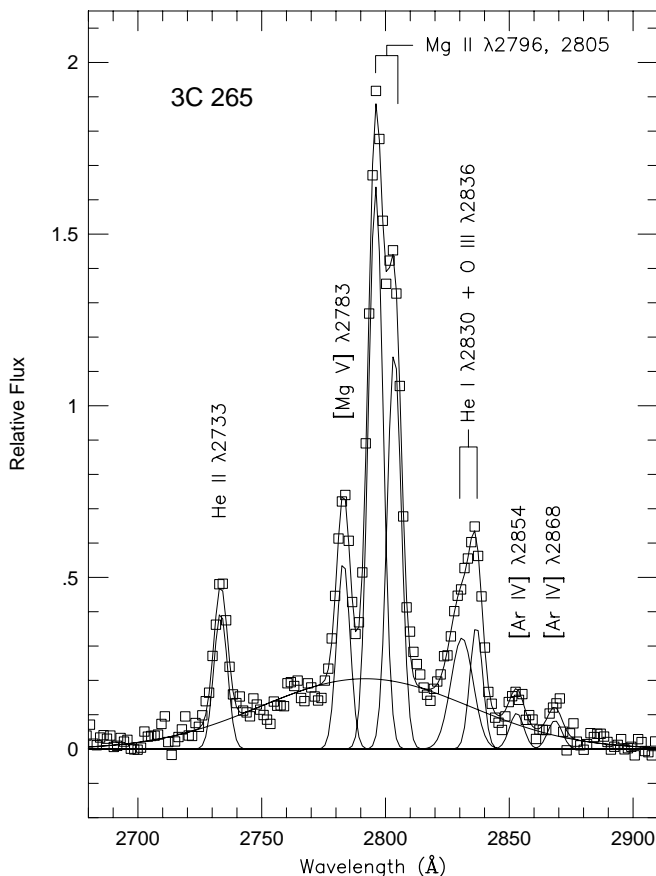


FIG. 2.—Fitting of Gaussian profiles to the Mg II emission-line complex of 3C 265 in total flux. The broad Mg II line has FWHM = $11,000 \pm 700 \text{ km s}^{-1}$, which is consistent with that in $P \times F_{\lambda}$.

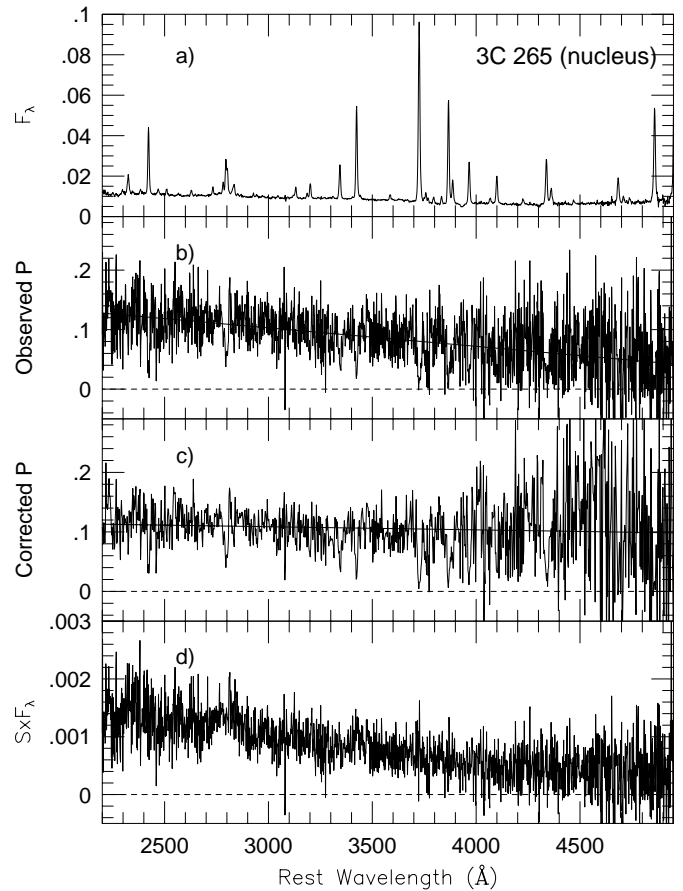


FIG. 3.—Spectropolarimetry of 3C 265 nucleus. (a) Total flux spectrum F_{λ} , (b) observed degree of polarization P , (c) P after correction for dilution by galactic host starlight, and (d) polarized flux spectrum $P \times F_{\lambda}$. The flux scales are in units of $10^{-15} \text{ ergs s}^{-1} \text{ cm}^{-2} \text{ \AA}^{-1}$. The smooth curves in (b) and (c) are straight-line fits to the continuum polarization. Note the presence of broad Mg II and lack of narrow emission lines in $P \times F_{\lambda}$. Note also that the increase in the observed P toward shorter wavelengths is flattened out in the corrected P spectrum (c).

trum $P \times F_{\lambda}$ (Fig. 3d; see also Cohen et al. 1996), demonstrating that the broad-line photons seen in the total flux spectrum are polarized, presumably by scattering of the light from an obscured nucleus. Note that the broad O III $\lambda 3444$ line also appears to be present in the $P \times F_{\lambda}$ spectrum of 3C 265 (Fig. 3d), which is similar to that observed in 3C 234 (Tran et al. 1995). By contrast, the narrow lines are essentially unpolarized, as evidenced by the sharp drop in P at these lines and their disappearance in the polarized flux spectrum, which has a relatively smooth, featureless continuum with spectral index $\alpha = 0$ ($F_{\nu} \propto \nu^{\alpha}$). The polarized broad Mg II line has a FWHM of about $12,000 \text{ km s}^{-1}$, which is consistent with that in the total flux spectrum. The average Mg II FWHM in radio-loud quasars is $4620 \pm 310 \text{ km s}^{-1}$ (with a range of 2000 – $10,000 \text{ km s}^{-1}$; Brotherton et al. 1994), so the measured width in 3C 265 is significantly above average. This is most simply interpreted as being due to additional thermal broadening by the scattering plasma, a possibility that will be discussed further in § 4.3. The polarization P.A. is featureless and constant with wavelength with a mean of 30° .

In addition to the strong emission lines that are seen, absorption features due to Ca II K at 3934 \AA and the G band at 4301 \AA are clearly present in the nuclear spectrum

of 3C 265 (see Fig. 1), indicating a significant presence of galaxian starlight. If these absorption features are due to a normal population of cool stars as found in typical nearby elliptical galaxies, then the contribution of this galaxy component to the total observed flux is about $f_G = 50\%$ at $\sim 4100 \text{ \AA}$, dropping to near zero at 2200 \AA , based on the galaxy subtraction method described by Tran (1995a) using NGC 821 as a template. This starlight fraction is in excellent agreement with the modeling results of di Serego Alighieri et al. (1996). The rest frame EW of the Ca II K absorption line in the nuclear spectrum of 3C 265 is $4.1 \pm 0.5 \text{ \AA}$, which is comparable to the value of $5.5 \pm 0.5 \text{ \AA}$ measured by Dey & Spinrad (1996). Assuming that the starlight is entirely unpolarized, we corrected the observed P for dilution and obtained an intrinsic polarization that is independent of wavelength to within the uncertainties (Fig. 3c).

It is of great interest to see if similar absorption-line features are present in the off-nuclear spectra of the extended emission regions or “knots.” Detection of these features in the extensions would provide conclusive evidence for the presence of starlight being directly associated with these extensions, as would be expected in the jet-induced star formation hypothesis. On the other hand, failure to detect these absorption features in the optical/UV would not necessarily rule out this scenario, since the star formation regions could be dominated by light from hot, young stars which lack these absorption features. The spectra of the northwest and southeast extensions of 3C 265 are shown in Figure 4. The northwest spectrum was extracted from a spatial region $5''.8$ wide along the slit, and that of the southeast knot covered a region $3''.2$ wide along the slit. These spectra do not show evidence for any absorption lines, but they have significantly lower S/Ns than the nuclear spectrum. Higher S/N data are needed to conclusively rule out the presence of absorption lines. However, broad Mg II is detected in these spectra, which is consistent with the finding of Dey & Spinrad (1996) and indicates that scattered nuclear light from an obscured broad-line active galactic nucleus (AGN) is present in the extensions. The high polarizations observed for these knots (Cohen et al. 1996; also see below) strengthen this view.

Close inspection of the off-nuclear spectra of 3C 265 reveals that the northwest and the southeast knots have different velocity profiles. In the northwest, the narrow emission lines are fairly symmetrical and redshifted relative to the nucleus, while in the southeast, they are blueshifted and have a blue-wing asymmetry *plus* a weak red wing. Figure 5 illustrates these differences for the profile of the [O II] $\lambda 3727$ emission line. The projected velocity shifts relative to the nucleus are $\sim +120 \text{ km s}^{-1}$ for the northwest and -190 km s^{-1} for the southeast knot. In addition, the Balmer continuum discontinuity and high- n emission lines appear stronger in the northwest spectrum than in the southeast spectrum (Fig. 4). Detailed analysis of the line strengths is given in a separate paper, but we note here that these velocity shifts imply that if there is an outflow of material in the two sides of the cone, the northwest lobe would be behind the southeast lobe. VLBI observations of the inner core to look for any jet/counterjet flux enhancement resulting from Doppler boosting would be useful for confirmation. Alternatively, the line shifts could simply be due to rotation or inflow. The origin of the line asymmetry and its difference between the two sides are not understood but could possibly be due to dust obscuration.

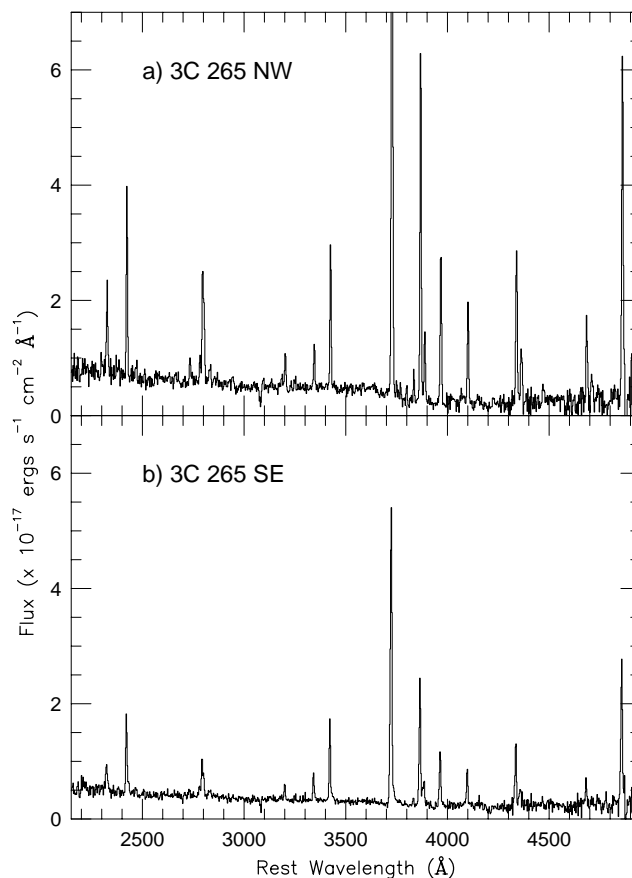


FIG. 4.—Off-nuclear spectra of the northwest and southeast emission-line extensions of 3C 265. (a) The northwest extension; (b) the southeast extension. Note the lack of the Ca II K and G band stellar absorption feature, which indicates the lack of a concentration of old stars in these regions. Broad Mg II is present at a low level.

The imaging polarimetry of 3C 265 obtained through a V filter is displayed in Figure 6. This shows clearly the double lobes of highly polarized radiation, which are spatially coincident with the extended UV/optical emission. The polarization electric vectors are closely perpendicular to the radio axis in the inner regions close to the nucleus (for radio maps, see Leahy, Muxlow, & Stephend 1989 and Fernini et al. 1993). In the outer extents, although the extended emission line regions (EELR) in this galaxy do not align well with the radio axis, the polarization vectors are well aligned with the EELR and perpendicular to the radius vector from the central flux peak. To quantify this perpendicular relationship, we examine the angle between a line joining the flux peak to each electric vector and the perpendicular to it. The mean deviation of this angle for 53 vectors (excluding those in a 7×7 box around the nucleus which are contaminated by seeing and spatial averaging) is -1.4 ± 1.1 . This remarkably tight distribution demonstrates that scattering must be entirely responsible for the polarization and that the nuclear source for the scattered light must lie close to the flux peak. In addition, there is a general *increase* in P with radius throughout the spatially extended regions (see Table 1 of Cohen et al. 1996; see also Cimatti et al. 1996; Dey et al. 1996). We discuss the implications of these results in § 4.2. Our observations confirm the results of Jannuzi & Elston (1991), who detected a similar level of polarization and orientation of the electric vectors with respect to the extended optical/radio morphology.

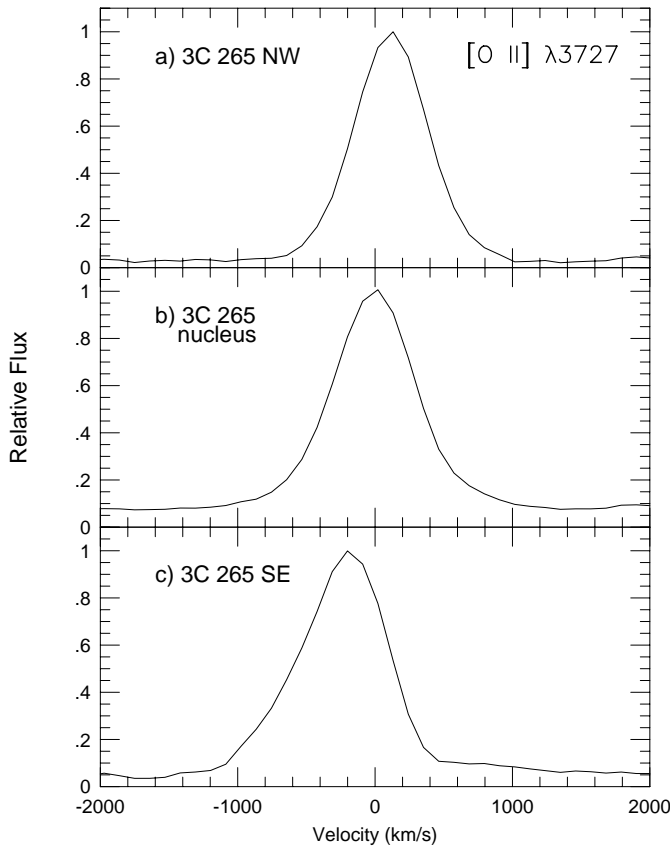


FIG. 5.—Emission-line profile of [O II] $\lambda 3727$ in the (a) northwest, (b) nucleus, and (c) southeast regions of 3C 265 to illustrate the differences in velocity profiles and shifts among the three components.

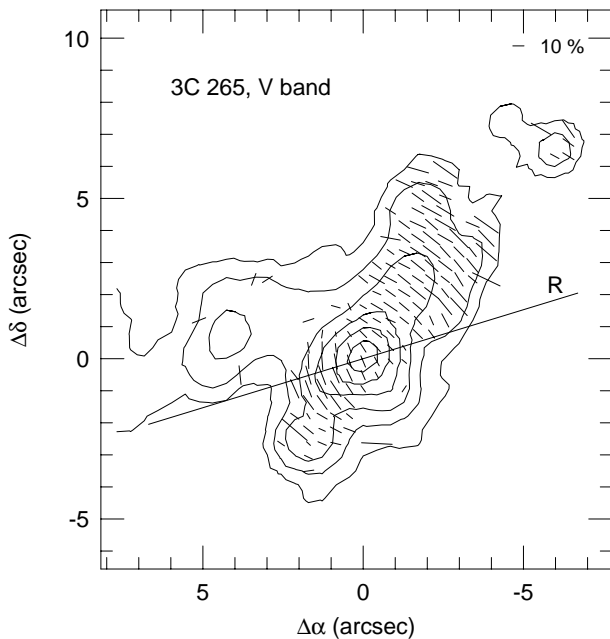


FIG. 6.—V-band imaging polarimetry of 3C 265. Polarization vectors are superimposed on the total intensity contours. Contours are 2%, 4%, 8%, 16%, 32%, and 64% of peak intensity. In this and all subsequent polarimetric images, only vectors whose S/N > 2 are plotted; north is up, and east is to the left. The data have been binned 2×2 , giving an effective scale of $0.43'' \text{ pixel}^{-1}$. The solid line marked with an R indicates the orientation of the radio axis. The extended emission regions are highly polarized, with P.A. perpendicular to the radius vectors and the degree of polarization generally increasing with radius from the central nucleus. The radio axis (R) is not aligned with the UV/optical extensions in this object.

3.2. 3C 277.2

The spectropolarimetry of 3C 277.2 ($z = 0.763$) is shown in Figure 7. Like 3C 265, the radiation is highly polarized, reaching $\sim 30\%$ in the blue (rest frame UV). The observed polarization displays a smooth rise to the blue as in 3C 265, but like the latter, this is most likely due to the decreasing effect of starlight dilution. Stellar absorption lines from the host galaxy are also seen. Unfortunately, the Ca II K line and G band fall fortuitously on the B and A atmospheric bands, respectively, making the determination of the relative contribution of the galaxy component to the total observed flux more problematic and far less reliable. It appears, however, that the starlight fraction is less than that in 3C 265. Averaged over 4100–5100 Å (observed wavelength), the observed polarization is $29\% \pm 6\%$, which is consistent with the value of $21\% \pm 4\%$ reported by di Serego Alighieri et al. (1989) in the B band. The polarization P.A. is independent of wavelength, with a mean of 168° . This is 73° from the radio structure axis of 61° (McCarthy et al. 1987; see Pedelty et al. 1989 and Leahy et al. 1989 for radio maps). The narrow lines are essentially unpolarized, as evidenced by the sharp drop of P in these lines and their absence in $P \times F_\lambda$. These characteristics, including the high magnitude of polarization and constancy of P and P.A. with wavelength, suggest that scattering is the main mechanism responsible for the observed polarization. $P \times F_\lambda$ appears featureless with only a smooth continuum rising slightly

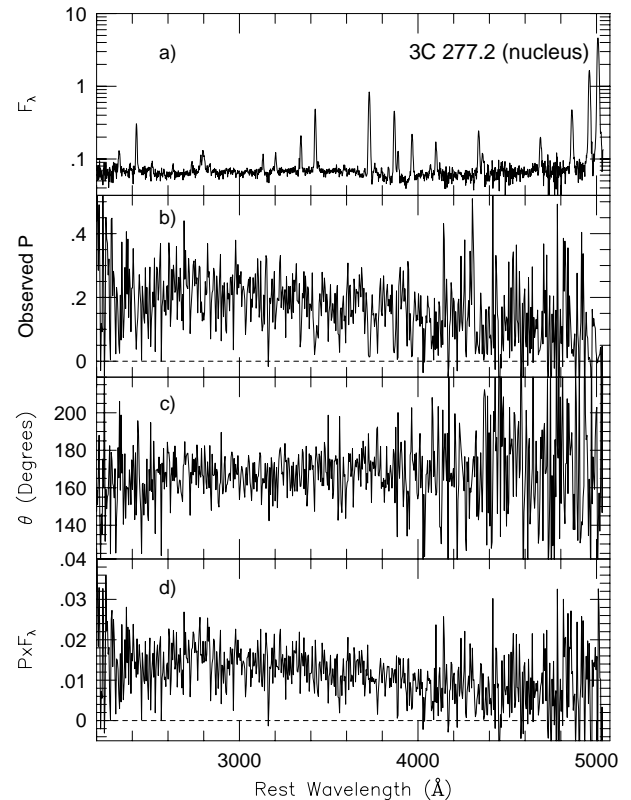


FIG. 7.—Spectropolarimetry of 3C 277.2 nucleus. (a) Total flux spectrum (F_λ plotted in logarithmic scale), (b) observed degree of polarization P , (c) polarization position angle θ , and (d) polarized flux spectrum $P \times F_\lambda$. The flux scales are in units of $10^{-16} \text{ ergs s}^{-1} \text{ cm}^{-2} \text{ \AA}^{-1}$. All data except F_λ in (a) have been binned by 3 pixels in wavelength to improve S/N. Broad Mg II line is evident in the total flux spectrum, although it is not as obvious in $P \times F_\lambda$. Stellar absorption line features and the Balmer discontinuity around 3650 Å are also present. The narrow lines are unpolarized.

toward the UV, showing no obvious sign of broad Mg II. The S/N, however, is poorer than in 3C 265, and any broad lines present might be lost in the noise and be difficult to detect. However, a broad component of Mg II is easily discernible in the total flux spectrum (Fig. 8). Fitting a Gaussian profile to this component gives a FWHM of $13,000 \pm 1500 \text{ km s}^{-1}$, which is similar to that of 3C 265 and indicates that it too could be thermally broadened by the scatterers.

Like 3C 265, the spectrum of 3C 277.2 shows emission lines of a wide range of ionization and atomic species. Most of the lines identified in 3C 265 are observed in 3C 277.2, and their measured line ratios are listed in Table 2. The weakness of any broad-line components in $P \times F_\lambda$ prevents us from estimating the strength of any unpolarized second featureless continuum (FC2) (Tran 1995c), but it appears (due to the higher P) that any FC2 present is weak compared to that in 3C 265 (see § 4.1). These results suggest that 3C 277.2 represents another case of a quasar hidden from direct view in a normal radio galaxy, and they thus support the radio galaxy/quasar unification hypothesis (Barthel 1989).

A polarization map of 3C 277.2 obtained with a V filter is shown in Figure 9. The EELR is less extended than in 3C 265, but the polarization is high near the nucleus.

3.3. 3C 324

Keck spectropolarimetry of 3C 324 ($z = 1.206$) has recently been discussed by Cimatti et al. (1996). We present the B -band imaging polarimetry of this object in Figure 10.

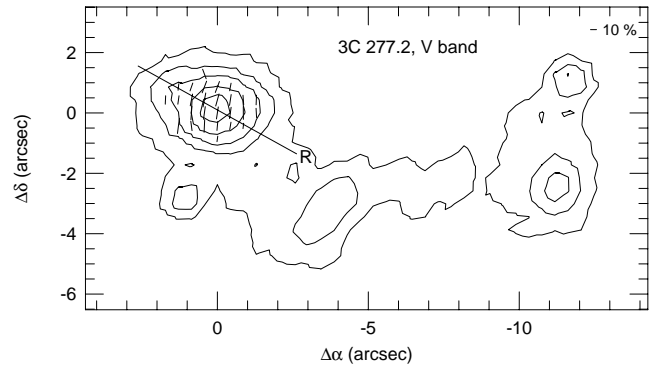


FIG. 9.— V -band imaging polarimetry of 3C 277.2. Contours are 2%, 5%, 10%, 25%, and 60% of peak intensity. Displayed as in Fig. 6, except the cutoff for vectors plotted is at 2.5σ instead of 2σ . High, significant polarization is detected near the nucleus. P is fairly constant throughout in the detectable regions and does not show the P gradient seen in 3C 265 and 3C 324. There are some extended emission regions to the west, whose polarization is below the detection limit of this image ($P < 4\%$, 2σ).

The polarization level is high throughout much of the nuclear and extended emission regions, with P.A. roughly perpendicular to the radio/extended optical structure axis (VLA radio maps of the source can be found in Pedelty et al. 1989 and Fernini et al. 1993). The level of the observed polarization in the nucleus ($12\% \pm 1.3\%$) is consistent with the measurements of Cimatti et al. (1996) ($\sim 11\%$). Again, the rise in P in the outer parts of the galaxy is present,

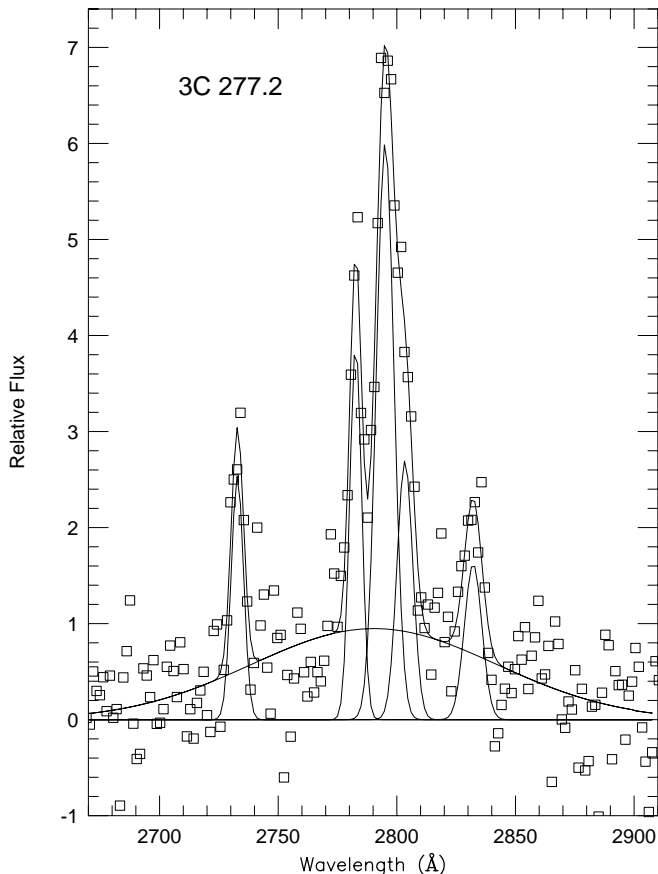


FIG. 8.—Fitting of Gaussian profiles in the total flux emission-line complex of Mg II in 3C 277.2. The broad Mg II line has $\text{FWHM} = 13,000 \pm 1500 \text{ km s}^{-1}$, which is similar to that of 3C 265.

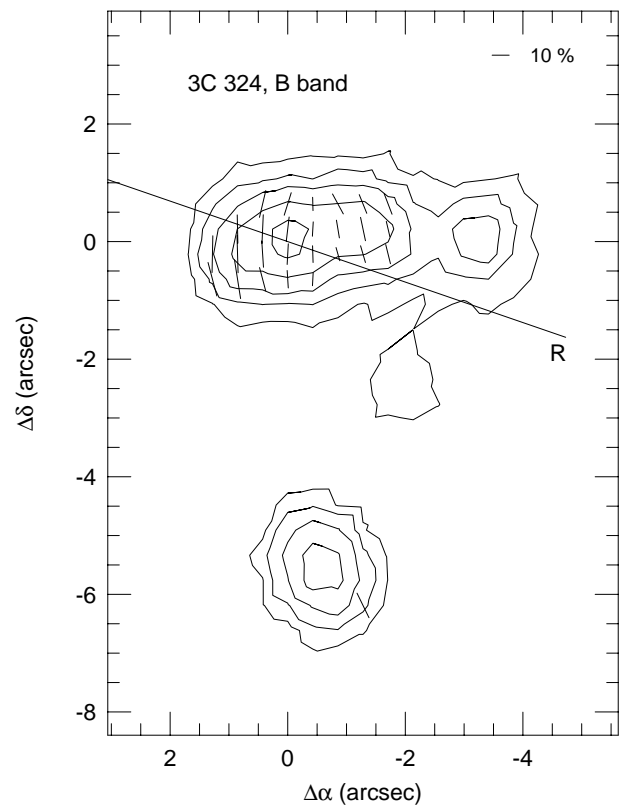


FIG. 10.— B -band imaging polarimetry of 3C 324, displayed as in Fig. 6. Contours are 10%, 17%, 29%, 49%, and 83.5% of peak intensity. P shows a slight increase from the nucleus to the eastern but not the western extension. The component $\sim 3''$ to the west of the nucleus is essentially unpolarized, which suggests that it is an independent galaxy dominated by starlight.

especially toward the east, similar to that observed in 3C 265. These results confirm those reported by Cimatti et al. (1996) with their long-slit data. The apparent “extended lobe” ~ 3.3 to the west of the nucleus is essentially unpolarized. It is most likely an interacting/merging or companion galaxy at a redshift similar to that of 3C 324 (Cimatti et al. 1996).

3.4. 3C 343.1

In contrast to 3C 265 and 3C 277.2, the nuclear flux spectrum of 3C 343.1 ($z = 0.750$, Fig. 11) is characterized by the weakness or absence of higher ionization lines like [Ne v] or He II and by the presence of easily detectable broad wings at H β , H δ , and probably Mg II. In addition, the absorption line spectrum is dominated by a younger population of stars, as can be seen by the prevalence of absorption lines due to high- n Balmer lines, the Balmer discontinuity, and the lack of a feature due to the G band that is characteristic of cooler stars seen in the 3C 265 and 3C 277.2 spectra. A most surprising finding, however, is that the redshift of the absorption lines is radically smaller ($z = 0.344$) than that of the nuclear AGN emission lines ($z = 0.75$)! As seen in Figure 11, the low-redshift system also contains emission lines, notably [O II] $\lambda 3727$ and [O III] $\lambda\lambda 4959, 5007$.

Examination of the two-dimensional spectroscopic data reveals that the [O II] $\lambda 3727$ emission line in the low- z emission-line galaxy is extended over $\sim 5''$, while the emission lines of [O II] and Mg II from the active nucleus are relatively compact. This demonstrates that the observed spectrum is composed of two different sources of radiation in a chance alignment. The distant object with $z = 0.75$ is the radio AGN 3C 343.1. The foreground object with $z = 0.344$ has a spectrum similar to that of the emission-line galaxy M51, showing the strong emission line of [O II] as well as strong absorption lines due to Ca II H and K and high- n Balmer lines (Fig. 11).

Based on the strength of [O II] relative to [O III], the foreground galaxy could be classified either as a LINER

(low-ionization nuclear emitting region; Heckman 1980) or starburst galaxy, although a measurement of [O I] $\lambda 6300$, which is lost in the high-noise region of the spectrum in the near-IR, is needed to establish its true classification. Nevertheless, the spectrum qualitatively appears much like that of M51, and we use the latter as a template to estimate the contamination to the nuclear spectrum of 3C 343.1 by the foreground galaxy. We find that the foreground galaxy contributes about 50% of the flux at the wavelength of Mg II, rising to nearly 70% at the wavelength of H β . Figure 12 shows the spectral decomposition. Thus, contamination of the 3C 343.1 spectrum is substantial, and any study of its intrinsic optical continuum must take this into account before interpretation can be made.

3C 343.1 is classified as a compact steep spectrum (CSS) radio source (see, e.g., Fanti & Spencer 1996). The VLA and VLBI radio images show a compact double structure with the two components separated by ~ 0.3 – 0.5 , extended east-west (van Breugel et al. 1992; Fanti et al. 1985). No polarization is detected at either 8.4 or 15 GHz (van Breugel et al. 1992; Akujor & Garrington 1995). In light of the fact that 3C 343.1 is closely aligned with a foreground galaxy at $z = 0.344$, the double morphology of the radio source could be a result of gravitational lensing. We note, however, that such morphology is rather common for CSS objects (see, e.g., Fanti et al. 1985), and no lensing may be involved. However, if this is a lens system, given the redshifts and radio separation, the mass of the foreground galaxy is estimated to be $\sim 3.5 \times 10^9 M_{\odot}$ (C. Fassnacht 1996, private communication). The similarity of the radio intensity ratios at 15 and 22.5 GHz between the two components in the VLA map (van Breugel et al. 1992) is consistent with their being a lensed system. Matching VLBI-scale structure and spectra in the radio images should be important in establishing whether or not this is indeed the case. The VLBI image of Fanti et al. (1985), however, shows very different shapes between the two components, so there is no strong evidence for lensing in the 3C 343.1 system. A recent *Hubble Space Telescope* (HST) snapshot survey of CSS radio sources by de Vries et al. (1997) does not reveal any peculiar

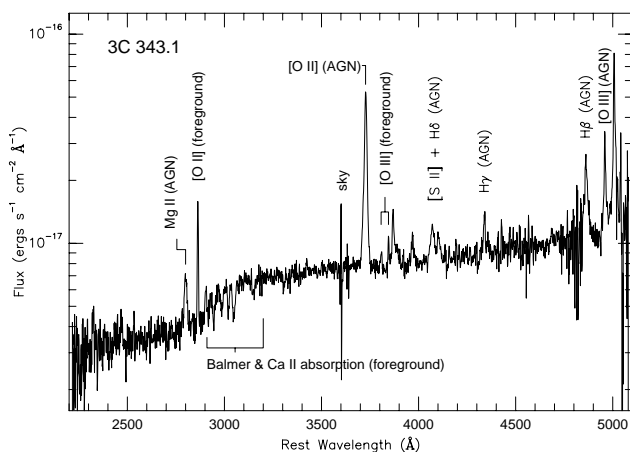


FIG. 11.—Observed total flux spectrum of 3C 343.1 nucleus, plotted in logarithmic scale to show the faint features and corrected for the redshift of the AGN. Note the presence of strong high- n Balmer absorption lines and broad wings in H β , H δ , and Mg II, as well as the lack of high ionization [Ne v] and He II lines. The absorption-line redshift is substantially lower ($z = 0.344$) than the emission-line redshift of the AGN nucleus ($z = 0.750$). There are also emission lines ([O II] and [O III]) at the same redshift as the absorption-line system.

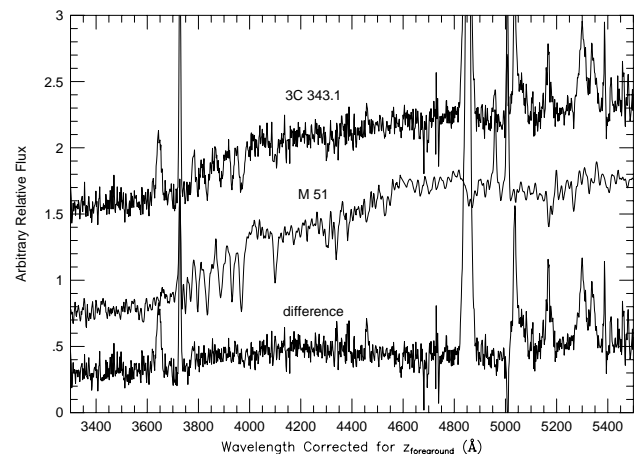


FIG. 12.—Decomposition of the nuclear spectrum of 3C 343.1 using M51 as a template. *Top*: Observed spectrum of 3C 343.1; *middle*: the spectrum of M51; *bottom*: the difference spectrum. For clarity, all spectra have been arbitrarily shifted vertically and corrected for the redshift of the absorption-line system $z = 0.344$ belonging to the foreground emission-line galaxy. It has a spectrum similar to that of M51 and makes up 50%–70% of the observed flux toward 3C 343.1.

structures in the field of 3C 343.1. Deeper *HST* imaging would be most informative and should help resolve the true structural morphology of this system.

Imaging observations in the light of the optical continuum and [O II] emission of the AGN by McCarthy et al. (1995) show a continuum structure slightly extended but offset 45° from that of the [O II] morphology, which is elongated east-west in the direction of the radio axis. The AGN [O II] emission has a $\sim 5''$ extent, similar to the extension of the [O II] emission in the foreground galaxy. Since we have shown that the optical continuum of 3C 343.1 is dominated by a foreground emission-line galaxy of similar spatial extent, it is easy to understand the observed misalignment between the continuum and [O II] morphologies of the radio galaxy and also why the optical emission in 3C 343.1 is extended well beyond the region of the radio emission (McCarthy et al. 1995). This property is not unique to 3C 343.1, but it is an extreme example. Because of the large distances and faint limiting magnitudes of these HzRGs, the chance alignment with a foreground source does not appear to be an uncommon occurrence. For example, the projection of a Galactic M dwarf within 1'' of the nucleus of 3C 368 has been reported by Hammer, Le Fèvre, & Proust (1991), and the superposition of a Galactic star with 3C 435B has been discussed by McCarthy, van Breugel, & Spinrad (1989). Furthermore, as there has been statistical evidence for an excess of foreground galaxies around HzRGs, presumably due to amplification bias caused by gravitational lensing (e.g., Hammer & Le Fèvre 1990; Benítez, Martínez-González, & Martín-Mirónes 1997), chance superpositions of these objects are to be expected.

We detect little polarization in the nucleus of 3C 343.1. The observed P integrated over the wavelength range 5000–7600 Å (observed) is $0.6\% \pm 1.6\%$ (uncorrected for the $z = 0.344$ galaxy). This is consistent with the upper limit of less than 9% reported by Tadhunter et al. (1992), but it is also consistent with zero. The presence of broad $H\beta$ and the lack of [Ne V] and He II, coupled with the observation that it is weakly or not polarized at all, would suggest that 3C 343.1 is a low-ionization broad-line radio galaxy viewed at a small inclination angle. The heavy contamination with a foreground, young emission-line galaxy further contributes to its lack of observed polarization. 3C 343.1 is also known as a CSS radio source, the polarization properties of which as a class have not been well studied, but recent evidence (Cohen et al. 1997) points to the intriguing possibility that the optical polarization of these sources comes from synchrotron radiation and is variable.

4. DISCUSSION

4.1. Total Flux Spectra and FC2

In 3C 265, the EW of the broad Mg II line is found to be significantly higher in $P \times F_\lambda$ than in the total flux (58 ± 3 Å compared to 12 ± 1 Å [rest frame], respectively). As mentioned by Cohen et al. (1996), this can be interpreted as being due to the presence of an unpolarized second featureless continuum, FC2, in the observed spectrum. This Mg II EW in $P \times F_\lambda$ is similar to those observed directly in normal quasars (Cristiani & Vio 1990), whereas in the hybrid Doppler-beamed continuum model, one would expect it to be much lower. Thus, any reflected Doppler-boosted component must be minimal in 3C 265. We can estimate the fraction of FC2 as (e.g., Tran 1995c):

$FC2/F_{\text{tot}} = 1 - EW(F_{\text{tot}})/EW(P \times F_\lambda) = 0.79$. The intrinsic polarization of the scattered component is then about 50%. Since the starlight component from an old stellar population of the host galaxy is expected to be insignificant at this wavelength, this FC2 appears to be related to, or the same as, that recently found in an increasing number of Seyfert 2 and radio galaxies (Tran 1995c; Tran et al. 1995; Dickson et al. 1995; Dey et al. 1996; Cimatti et al. 1996). An interesting possibility is that FC2 is due to hot stars being formed in the wake of the radio jets in the extranuclear regions (Longair, Best, & Röttgering 1995; Best et al. 1996). A radio jet interacting with the circumnuclear medium has been thought to induce star formation (e.g., Rees 1989), and this has been proposed to explain the alignment effect. If this is the case, hot stars in the extended regions could contribute a significant amount of UV light which could account for much, if not all, of the FC2. Signatures characteristic of stars in this spectral regions, such as the spectral breaks near 2600 and 2900 Å (Fanelli et al. 1992), could provide crucial information on this issue. However, such signatures are fairly weak for O, B type stars, and the additional presence of AGN light makes them difficult to detect conclusively. Searches for these features have been made in the spectra of 3C 256 and 3C 324, with inconclusive results. The observed continua are consistent both with a young stellar population and also with a nonstellar continuum (Dey et al. 1996; Cimatti et al. 1996). Similarly, the spectra of the off-nuclear knots in 3C 265 (Fig. 4) also show no significant sign of these breaks, which is consistent with either hot stars or nonstellar light.

Moderately hot stars (A type) could make their presence known from the high- n Balmer absorption lines. No such features are evident in the spectrum of 3C 265, although they may be impossible to detect because of the overlying Balmer emission lines. Young A-type starlight has been observed in 3C 343.1, but as shown in § 3.4, it comes from a foreground galaxy, not the host. However, many absorption features commonly associated with early-type galaxies, such as Ca II H and K lines, the 4000 Å break, and the G band are clearly seen (see Fig. 1). These features demonstrate the presence of cool, evolved stars, and thus the host galaxies of these sources have a “normal” character. Recent *HST* imaging of nearby quasars by Bahcall, Kirhakos, & Schneider (1995, 1996) has shown that luminous quasars occur in a great variety of host systems: from apparently normal elliptical and spiral galaxies to complex interacting components. If the hosts of these HzRGs are similar to those of quasars in the Bahcall sample, as may be the case since many radio galaxies have been shown to be quasars viewed from an unobstructed direction (e.g., this paper; Tran et al. 1995; Young et al. 1996; Dey et al. 1996; Cimatti et al. 1996, 1997), then the finding that some of them appear to be normal, evolved systems is consistent with the Bahcall et al. observations.

Alternatively, FC2 could simply represent the nebular continuum generated in situ in the emitting gas (Dickson et al. 1995), or it could be free-free thermal radiation from the scattering electrons themselves (Tran 1995c). For the latter to be valid, the scattering medium must be dominated by electrons and not dust. Nebular continua are detected in both the nuclear and off-nuclear (northwest) spectra of 3C 265 (Figs. 1 and 4) and in the spectrum of 3C 277.2 (Fig. 7), based on the presence of the Balmer discontinuity around 3650 Å. Careful examination of the scattering mechanism

should provide important insights into the origin of this FC2 component. The recognition of FC2 in these galaxies means that it could make up part of the observable off-nuclear emission regions. If so, determination of the origin of this light would be of great value in understanding the alignment effect and the evolution of these galaxies as well as the nature of quasars in general. For example, *HST* images of the nearby luminous quasar PKS 2349-014 by Bahcall et al. (1995) have revealed a region of very diffuse and extended “nebulosity” surrounding the nucleus and extending up to ~ 40 pc. The origin and nature of this light is unknown. Similarly, an *HST* snapshot survey of Seyfert galaxies has revealed extended “fuzz” surrounding the nuclei of type 2, but not type 1, Seyfert galaxies (Nelson et al. 1996). If the quasars at the centers of these HzRGs are similar to PKS 2349-014, this faint extended nebulosity could represent a component of FC2 that dilutes the polarization. It could, for example, be tidal debris from galaxy interactions (e.g., Weil, Bland-Hawthorn, & Malin 1997). Further study of the host galaxies and FC2s of these HzRGs will shed light on the nature of this nebulosity in quasars.

4.2. Scattering versus Star Formation

In order to further investigate the geometry of the surrounding environments of HzRGs and to help address the question of scattering versus star formation, imaging polarization observations were obtained for 3C 265, 3C 324, and 3C 277.2. The results, shown in Figures 6, 9 and 10, reveal a number of interesting characteristics. First, the polarizations are all very high and consistent with the nuclear spectropolarimetry. Second, the polarization vectors, especially in 3C 265 (§ 3.1), show a double-lobed pattern that is centrosymmetric with respect to the nucleus and perpendicular to the radial vectors originating from it. Such bisymmetric fans of polarized light have also been observed in the nearby powerful NLRG Cyg A (Tadhunter, Scarrott, & Rolph 1990; Ogle et al. 1997). This is just what is expected from a simple geometry in which radiation from a compact obscured central source is scattered by the surrounding medium.

It is notable that the polarized light is spatially coincident with, and the polarization P.A. more closely orthogonal to, the UV extensions than the radio axis, as also discussed by Cimatti et al. (1996, and references therein) for many other radio galaxies. This phenomenon, in fact, has also been seen in Seyfert galaxies. For example, Tran (1995b) found that the polarization vectors in the luminous hidden quasar Mrk 463E are more perpendicular to the optical-UV extension (Uomoto et al. 1993) than to the radio structure axis, which suggests that the axis of symmetry of the scattering material lies along the optical extension and not the radio jet. The similar phenomenon in HzRGs suggests that scattering of light by material closely associated with the UV extensions rather than the jet is responsible for the observed perpendicular relationship. Moreover, it is interesting to note that in the case where the radio axis and UV extensions do not align well (e.g., 3C 265), this relationship also applies more with the UV extensions (see Fig. 6). This result clearly favors the scattering picture over jet-induced star formation as the main cause of the alignment effect. Di Serego Alighieri et al. (1996) have argued that the apparent misalignment between the radio axis and UV extensions in 3C 265 considerably weakens the case for star formation hypothesis because in

this picture, it is hypothesized that the radio jets trigger the star-forming process, and one would therefore expect a very close correspondence between the optical and radio structures in all cases.

The third notable characteristic displayed by the polarization images is that P shows a spatial gradient (most clearly seen in 3C 265) in the sense that its magnitude increases with increasing radial distance from the nucleus. This rise in the degree of polarization in the outer regions of HzRGs away from the nucleus has also been noted in both 3C 256 and 3C 324 by Dey et al. (1996) and Cimatti et al. (1996) in their one-dimensional spectropolarimetric data. Thus, it appears that this phenomenon is widespread if not universal among these objects. If the intrinsic polarization of the scattered light at every point in the galaxy is the same, this gradient in P may simply be due to the decreasing effect of dilution by diminishing unpolarized starlight at the outer regions of the galaxy, a characteristic suggested by Draper, Scarrott, & Tadhunter (1993). If radiation from luminous, young stars in their forming regions dominated in the extended emission regions, the opposite effect would be expected. Furthermore, it is unlikely that the gradient is caused by diminishing light from cool stars since the effect is seen in the observed V and B bands (~ 3000 Å rest frame), where radiation from such stars is not expected to dominate (e.g., Figs. 1 and 3). The ramification is that scattered light, not direct starlight, must increasingly dominate with radius in the extended regions. Again, this provides strong support for the scattered light hypothesis in explaining the alignment effect.

Another possibility is that near the nucleus, scattering takes place in an extended (three-dimensional) volume, so there is some cancellation of the P vectors, and the integrated polarization is reduced. At large distances, the scattering occurs mainly through large angles, and the polarization is correspondingly higher. Alternatively, the radial increase in P could be the result of a radial increase in scattering efficiencies and/or number of scatterers. How such differences in the scatterers’ properties could arise is not known. One intriguing possibility is that close to the nucleus, the polarization arises mainly from electron scattering, but farther out, it is dominated by dust scattering, which has higher scattering efficiency. An attractive feature of this picture is that it has been shown to operate in the nearby Seyfert galaxy NGC 1068 (Miller, Goodrich, & Matthews 1991). In this case, however, diagnostic signatures for dust scattering are clearly seen, while they have not been convincingly demonstrated in HzRGs (see, however, Knopp & Chambers 1997). In summary, imaging polarimetry provides convincing evidence that scattered radiation from an obscured nuclear source rather than star-forming regions dominates the extended emission in the HzRGs of this study.

4.3. Nature of the Scatterers

To address the question of the nature of the scatterers, one can first attempt to look at the intrinsic wavelength dependence of P . In § 3.1 we showed that the intrinsic polarization of 3C 265 is essentially wavelength independent and that the apparent rise of P toward the blue is due entirely to decreasing dilution by unpolarized starlight (Fig. 3c). The polarization P.A. is also wavelength independent. It is important to note that Dey et al. (1996) and Cimatti et al. (1996, 1997) also find that P and P.A. are essentially inde-

pendent of wavelength in 3C 13, 3C 256, and 3C 324. Although this is consistent with electron scattering, scattering by dust grains with the appropriate characteristics can just as well mimic the constancy of P and P.A. with wavelength (e.g., Kartje 1995; Manzini & di Serego Alighieri 1996). It is not possible, therefore, in the limited optical wavelength range, to discriminate between electron and dust scattering by examining the wavelength dependence of P alone.

One might expect that dust scattering may play a significant role in producing the observed polarization in these HzRGs. There has been evidence that dust must surely be present in many of these radio galaxies (Heckman, Chambers, & Postman 1992; Chini & Krügel 1994; Dey, Spinrad, & Dickinson 1995; Ivison 1995; Villar-Martín & Binette 1996, 1997), although there is no direct information on how it is spatially distributed. In addition, dust is much more efficient at scattering the light than electrons (by a factor of order $\sim 10^4$ in terms of scattering cross section per unit mass). In fact, in many cases it has been thought to be the main or dominant process responsible for the observed polarization (Cimatti et al. 1993; di Serego Alighieri et al. 1994; Manzini & di Serego Alighieri 1996; Knopp & Chambers 1997).

Some arguments against dust include the lack of any sharp rise in P in the UV for $\lambda \lesssim 2500 \text{ \AA}$, as would be expected from theoretical predictions regardless of the grain size, composition, and distribution (Kartje 1995; Manzini & di Serego Alighieri 1996). In addition, observable signatures that are indicative of dust scattering, such as the extreme blueness ($\alpha \sim +2$) of the polarized, scattered continuum (Cyg A: Ogle et al. 1997; NGC 7674: Miller & Goodrich 1990; Tran 1995b) and the lack of any significant broadening of permitted lines in $P \times F_\lambda$ spectrum (NGC 7674: Miller & Goodrich 1990; Tran 1995b; the northeast knot in NGC 1068: Miller et al. 1991), have not been seen in many HzRGs observed so far. The spectral index of $P \times F_\lambda$ in 3C 265 is $\alpha = 0$, and in 3C 277.2, $\alpha = -0.2$. These values are consistent with the typical spectral slopes of normal QSOs (Francis et al. 1991; Natali et al. 1998) with no significant “blueing,” which suggests that some type of gray scatterers may more likely be responsible. The lack of any observable polarization or spectral flux signatures associated with the 2175 Å “bump” of the interstellar extinction curve is also puzzling, although the composition, size distribution, and extinction properties of the dust in these galaxies could be very different from those in our Galaxy. For example, the extinction curves of the Small Magellanic Cloud and of starburst galaxies lack such a 2175 Å dust feature (Prévot et al. 1984; Calzetti, Kinney, & Storchi-Bergmann 1994; Gordon, Calzetti, & Witt 1997; Rodrigues et al. 1997). Also, Manzini & di Serego Alighieri (1996) have argued that it is possible to reduce the strength of this signature in the scattered flux by introducing an appropriate amount of extinction in addition to scattering. Such a process may also help explain the lack of any strong blueing in the observed scattered spectra.

Electrons are thought to be the dominant scattering agent in Seyfert galaxies⁵ (e.g., Miller et al. 1991; Tran 1995b), albeit at spatial scales much closer to the nucleus (\lesssim a few parsecs) than those associated with the HzRGs

described here (\sim tens of kiloparsecs). One clue that argues in favor of electron scattering in 3C 265 and 3C 277.2 is the broadening of the Mg II line in $P \times F_\lambda$ (§§ 3.1, 3.2). The magnitude of the broadening is such that if electrons were the scatterers, the temperature of the plasma clouds is $\sim 5 \times 10^5 \text{ K}$, not hot enough to smear out the line completely but comparable to the temperature found for the scattering electrons in NGC 1068 (Miller, Goodrich, & Mathews 1991). Of the previous HzRGs that have been observed, we note that in 3C 256, 3C 324, and 3C 356, electron scattering could not be ruled out by the data and might even be slightly favored in 3C 256 (Jannuzi et al. 1995; Dey et al. 1996; Cimatti et al. 1996, 1997).

This leads us to conclude that while there is no doubt that dust is present in these galaxies and most probably responsible to some extent for the scattered light, electron scattering also contributes significantly, despite its lower scattering efficiency. The only main argument against electron scattering is the uncomfortably large mass of ionized gas ($\sim 10^9\text{--}10^{12} M_\odot$, see, e.g., Dey et al. 1996) that would be required because of the large spatial scales involved. Nevertheless, if electron scattering is the dominant process, it is difficult to attribute the alignment effect to star-forming regions alone, as one would expect scattering by dust that is abundant in the molecular clouds from which stars form might dominate. As discussed by Dey et al. (1996), another consequence of the electron-dominated scattering picture is the implication for a dust-to-gas ratio in the interstellar medium of these galaxies that is smaller than that of our Galaxy. Although the issue is far from resolved, recent evidence suggests that the amount of dust in high-redshift galaxies (Pettini et al. 1997) appears to always be smaller than in the Milky Way, which is consistent with the above conclusion.

5. SUMMARY AND CONCLUSIONS

The main observational results of this paper are as follows:

1. Broad permitted emission lines (Mg II) are observed in $P \times F_\lambda$ (3C 265) and total flux (3C 265 and 3C 277.2).
2. The widths of the Mg II lines in F_λ (3C 265 and 3C 277.2) and $P \times F_\lambda$ (3C 265) are extraordinarily large compared to normal, radio-loud quasars. A similar broadening is also observed in 3C 324 and 3C 356 (Cimatti et al. 1996, 1997).
3. The P and P.A. are generally constant with wavelength, after dilution by host starlight is taken into account. This appears to be a common phenomenon in many HzRGs (e.g., 3C 13, 3C 277.2, 3C 256, 3C 265, and 3C 324).
4. Polarization P.A.’s are perpendicular to the UV extensions and, perhaps more importantly, to the overall radial structure of the galaxy. P levels are generally high and comparable to those in Seyfert galaxies.
5. Imaging polarimetry of 3C 265 shows that the P vectors display a centrosymmetric pattern with respect to the nucleus, with magnitudes that generally increase radially outward from the nucleus into the extended emission regions.
6. Spectroscopically, P shows a slight increase in the wings of broad emission lines (e.g., Mg II) compared to the continuum, or equivalently, $\text{EW}(P \times F_\lambda) > \text{EW}(\text{total flux})$, as has been seen in Seyfert 2 galaxies and the radio galaxy 3C 234 (Tran 1995c; Tran et al. 1995).

⁵ The situation for Seyfert 1 galaxies is less clear, but both electrons and dust are thought to contribute (Goodrich & Miller 1994).

7. Narrow emission lines are unpolarized, which suggests that the scattering material is primarily inside of, or coincides spatially with, the emitting gas of the EELR.

8. Emission-line spectra of 3C 265 and 3C 277.2 are rich in a wide range of ionization and atomic species. Nebular continua are detected in the nuclear and off-nuclear spectra of 3C 265 and 3C 277.2. No stellar absorption lines are detected in the off-nuclear extensions, although the present S/N is poor. Better quality data are needed to examine this issue more closely and provide a definitive statement.

9. Host galaxies in HzRGs appear to be normal (evolved) elliptical galaxies or spiral bulges with a population of cool, evolved stars, based on the success of a normal elliptical template in decomposing the observed spectra.

10. 3C 343.1 is found to be a superposition of two galactic systems along the line of sight; one is a radio AGN at high redshift, and the other is a foreground, emission-line galaxy containing a young stellar population.

Results 1–9 provide strong support for the hidden quasar hypothesis and the unification of radio galaxies and quasars based on orientation. They indicate the presence of an unpolarized extended continuum component of the UV light, FC2, which has a decreasing contribution in the extensions, causing P to rise there compared to the nucleus. Together with the centrosymmetric fan of polarized light around the nucleus, this clearly shows that scattered light from a central obscured source dominates the extended emission regions and argues against the jet-induced star formation hypothesis as the main cause of the alignment effect. Scattering of Doppler-boosted light from a relativistic jet cannot be the dominant effect in these objects, since we see broad Mg II in $P \times F_{\lambda}$ with an EW comparable with that observed directly in normal (nonblazar) quasars. FC2 could be hot stars, the nebular continuum, or another component that might be related to the “diffuse nebulosity” observed in *HST* images of quasars. Another possibility to explain the radial P gradient is that the scattering in the nucleus is dominated by electrons (less efficient), while in the outer extensions, it is dominated by dust (more efficient). However, no common optical/UV

polarimetric signatures for the latter, such as a rapid rise of P with shorter wavelength or an extremely blue polarized continuum as observed for the types of dust grains in our Galaxy and other Seyfert galaxies, have been seen in HzRGs as a class. While previous works have suggested evidence for a large amount of dust in HzRGs and scattering by this dust cannot be entirely ruled out by polarimetric data, there is evidence that electron scattering plays a significant and perhaps major role in producing the polarized light observed in these galaxies. Along with the studies of Dey et al. (1996) and Cimatti et al. (1996, 1997), these conclusions apply well to those HzRGs at $z \sim 1$ that are highly polarized. There are indications that at much higher redshifts, the situation may be very different, with star-forming regions dominating the extended light (e.g., Dey et al. 1997), implying cosmological evolution of distant radio galaxies.

The W. M. Keck Observatory is operated as a scientific partnership between the California Institute of Technology and the University of California. It was made possible by the generous financial support of the W. M. Keck Foundation. We are grateful to Tom Bida for assistance with the observations and to A. Martel for assistance with some of the reduction. We thank D. E. Osterbrock for useful discussions and for his help with the identification of some of the emission lines. We thank an anonymous referee whose suggestions clarified several points. Work performed at the IGPP/LLNL is supported by the Department of Energy under contract W7405-ENG-48. During the course of this work, H. D. T. was supported by postdoctoral research fellowships at the California Institute of Technology through NSF grant AST 91-21889 and at Lick Observatory through grant AST 88-18925. S. S. A. thanks Caltech for hospitality during this work. This research has made use of the NASA/IPAC Extragalactic Database (NED) which is operated by the Jet Propulsion Laboratory, Caltech, under contract with the National Aeronautics and Space Administration.

REFERENCES

- Akujor, C. E., & Garrington, S. T. 1995, *A&AS*, 112, 235
 Antonucci, R. R. J. 1984, *ApJ*, 278, 499
 Antonucci, R. R. J., & Miller, J. S. 1985, *ApJ*, 297, 621
 Bahcall, J. N., Kirhakos, S., & Schneider, D. P. 1995, *ApJ*, 447, L1
 ———. 1996, *ApJ*, 457, 557
 Barthel, P. D. 1989, *ApJ*, 336, 606
 Benítez, N., Martínez-González, E., & Martín-Mirónes, J. M. 1997, *A&A*, 321, L1
 Best, P. N., Longair, M. S., & Röttgering, H. J. A. 1996, *MNRAS*, 280, L9
 ———. 1997, *MNRAS*, 286, 785
 Brotherton, M. S., Wills, B. J., Steidel, C. C., & Sargent, W. L. W. 1994, *ApJ*, 423, 131
 Calzetti, D., Kinney, A. L., & Storchi-Bergmann, T. 1994, *ApJ*, 429, 582
 Chambers, K. C., Miley, G. K., & Joyce, R. R. 1988, *ApJ*, 329, L75
 Chini, R., & Krügel, E. 1994, *A&A*, 288, L33
 Cimatti, A., di Serego Alighieri, S., Fosbury, R. A. E., Salvati, M., & Taylor, D. 1993, *MNRAS*, 264, 421
 Cimatti, A., Dey, A., van Breugel, W., Antonucci, R., & Spinrad, H. 1996, *ApJ*, 465, 145
 Cimatti, A., Dey, A., van Breugel, W., Hurt, T., & Antonucci, R. 1997, *ApJ*, 476, 677
 Cohen, M. H., Tran, H. D., Ogle, P. M., & Goodrich, R. W. 1996, in *IAU Symp. 175, Extragalactic Radio Sources*, ed. R. Ekers, C. Fanti, & L. Padrielli (Dordrecht: Kluwer), 223
 Cohen, M. H., Vermeulen, R. C., Ogle, P. M., Tran, H. D., & Goodrich, R. W. 1997, *ApJ*, 484, 193
 Cristiani, S., & Vio, R. 1990, *A&A*, 227, 385
 Daly, R. A. 1992, *ApJ*, 386, L9
 de Vries, W. H., et al. 1997, *ApJS*, 110, 191
 Dey, A., Cimatti, A., van Breugel, W., Antonucci, R., & Spinrad, H. 1996, *ApJ*, 465, 157
 Dey, A., & Spinrad, H. 1996, *ApJ*, 459, 133
 Dey, A., Spinrad, H., & Dickinson, M. 1995, *ApJ*, 440, 515
 Dey, A., van Breugel, W., Vacca, W. D., & Antonucci, R. 1997, *ApJ*, 490, 698
 De Young, D. S. 1981, *Nature*, 293, 43
 ———. 1989, *ApJ*, 342, L59
 Dickson, R., Tadhunter, C., Shaw, M., Clark, N., & Morganti, R. 1995, *MNRAS*, 273, L29
 di Serego Alighieri, S., Cimatti, A., & Fosbury, R. A. E. 1994, *ApJ*, 431, 123
 di Serego Alighieri, S., Cimatti, A., Fosbury, R. A. E., & Perez-Fournon, I. 1996, *MNRAS*, 279, L57
 di Serego Alighieri, S., Fosbury, R. A. E., Quinn, P. J., & Tadhunter, C. N. 1989, *Nature*, 341, 307
 Draper, P. W., Scarrott, S. M., & Tadhunter, C. N. 1993, *MNRAS*, 262, 1029
 Fanelli, M. N., O’Connell, R. W., Burstein, D., & Wu, C.-C. 1992, *ApJS*, 82, 197
 Fanti, C., Fanti, R., Parma, P., Schilizzi, R. T., & van Breugel, W. J. M. 1985, *A&A*, 143, 292
 Fanti, R., & Spencer, R. E. 1996, in *IAU Symp. 175, Extragalactic Radio Sources*, ed. R. Ekers, C. Fanti, & L. Padrielli (Dordrecht: Kluwer), 63
 Fermi, I., Burns, J. O., Bridle, A. H., & Perley, R. A. 1993, *AJ*, 105, 1690
 Francis, P. J., Hewett, P. C., Foltz, C. B., Chaffee, F. H., Weymann, R. J., & Morris, S. L. 1991, *ApJ*, 373, 465
 Goodrich, R. W., & Cohen, M. H. 1992, *ApJ*, 391, 623
 Goodrich, R. W., & Miller, J. S. 1994, *ApJ*, 434, 82
 Gordon, K. D., Calzetti, D., & Witt, A. N. 1997, *ApJ*, 487, 625

- Hammer, F., & Le Fèvre, O. 1990, *ApJ*, 357, 38
Hammer, F., Le Fèvre, O., & Proust, D. 1991, *ApJ*, 374, 91
Heckman, T. M. 1980, *A&A*, 87, 152
Heckman, T. M., Chambers, K. C., & Postman, M. 1992, *ApJ*, 391, 39
Ivison, R. J. 1995, *MNRAS*, 275, L33
Jannuzi, B. T., & Elston, R. 1991, *ApJ*, 366, L69
Jannuzi, B. T., Elston, R. E., Schmidt, G. D., Smith, P. S., & Stockman, H. S. 1995, *ApJ*, 454, L111
Kartje, J. F. 1995, *ApJ*, 452, 565
Knopp, G. P., & Chambers, K. C. 1997, *ApJ*, 487, 644
Leahy, J. P., Muxlow, T. W. B., & Stephens, P. W. 1989, *MNRAS*, 239, 401
Longair, M. S., Best, P. N., & Röttgering, H. J. A. 1995, *MNRAS*, 275, L47
Manzini, A., & di Serego Alighieri, S. 1996, *A&A*, 311, 79
McCarthy, P. J. 1993, *ARA&A*, 31, 693
McCarthy, P. J., Spinrad, H., & van Breugel, W. 1995, *ApJS*, 99, 27
McCarthy, P. J., van Breugel, W., & Spinrad, H. 1989, *AJ*, 97, 36
McCarthy, P. J., van Breugel, W. J. M., Spinrad, H., & Djorgovski, S. 1987, *ApJ*, 321, L29
Miller, J. S., & Goodrich, R. W. 1990, *ApJ*, 355, 456
Miller, J. S., Goodrich, R. W., & Mathews, W. G. 1991, *ApJ*, 378, 47
Natali, F., Giallongo, E., Cristiani, S., & La Franca, F. 1998, *AJ*, 115, 397
Nelson, C. H., MacKenty, J. W., Simkin, S. M., & Griffiths, R. E. 1996, *ApJ*, 466, 713
Ogle, P. M., Cohen, M. H., Miller, J. S., Tran, H. D., Fosbury, R. A. E., & Goodrich, R. W. 1997, *ApJ*, 482, L37
Oke, J. B., et al. 1995, *PASP*, 107, 375
Osterbrock, D. E. 1963, *Planet. Space Sci.*, 11, 621
———. 1997, in *Rev. Mexicana Astron. Astrofis.*, in press
Pedelty, J. A., Rudnick, L., McCarthy, P. J., & Spinrad, H. 1989, *AJ*, 97, 647
Pettini, M., King, D. L., Smith, L. J., & Hunstead, R. W. 1997, *ApJ*, 478, 536
Prévot, M. L., Lequeux, J., Maurice, E., Prévot, L., & Rocca-Volmerange, R. 1984, *A&A*, 132, 389
Rees, M. J. 1989, *MNRAS*, 239, 1P
Rodrigues, C. V., Magalhaes, A. M., Coyne, G. V., & Piirola, V. 1997, *ApJ*, 485, 618
Tadhunter, C. N., Scarrott, S. M., Draper, P., & Rolph, C. 1992, *MNRAS*, 256, 53P
Tadhunter, C. N., Scarrott, S. M., & Rolph, C. D. 1990, *MNRAS*, 236, 163
Tran, H. D. 1995a, *ApJ*, 440, 565
———. 1995b, *ApJ*, 440, 578
———. 1995c, *ApJ*, 440, 597
Tran, H. D., Cohen, M. H., & Goodrich, R. W. 1995, *AJ*, 110, 2597
Uomoto, A., Caganoff, S., Ford, H. C., Rosenblatt, E. I., Antonucci, R. R. J., Evans, I. N., & Cohen, R. D. 1993, *AJ*, 105, 1308
van Breugel, W. J. M., Fanti, C., Fanti, R., Stanghellini, C., Schilizzi, R. T., & Spencer, R. E. 1992, *A&A*, 256, 56
Villar-Martín, M., & Binette, L. 1996, *A&A*, 309, 97
———. 1997, *A&A*, 317, 350
Weil, M. L., Bland-Hawthorn, J., & Malin, D. F. 1997, *ApJ*, 490, 664
Young, S., Hough, J. H., Efstathiou, A., Wills, B. J., Axon, D. J., Bailey, J. A., & Ward, M. J. 1996, *MNRAS*, 279, L72